Quantum critical point revisited by dynamical mean-field theory

Wenhu Xu, Gabriel Kotliar, and Alexei M. Tsvelik

Quantum Critical Point revisited by the Dynamical Mean Field Theory

Wenhu Xu,[1] Gabriel Kotliar,[1,2] and Alexei M. Tsvelik[1]

[1]*Division of Condensed Matter Physics and Material Science,*
Brookhaven National Laboratory, Upton, NY 11973
[2]*Department of Physics and Astronomy, Rutgers University, Piscataway, NJ 08854*

Dynamical mean field theory is used to study the quantum critical point (QCP) in the doped Hubbard model on a square lattice. The QCP is characterized by a universal scaling form of the self energy and a spin density wave instability at an incommensurate wave vector. The scaling form unifies the low energy kink and the high energy waterfall feature in the spectral function, while the spin dynamics includes both the critical incommensurate and high energy antiferromagnetic paramagnons. We use the frequency dependent four-point correlation function of spin operators to calculate the momentum dependent correction to the electron self energy. By comparing with the calculations based on Spin-Fermion model, our results indicate the frequency dependence of the the quasiparitcle-paramagnon vertices is an important factor to capture the momentum dependence in quasiparticle scattering.

Introduction. The interplay between quasiparticles and bosonic collective modes, in particular in the proximity of a quantum critical point (QCP)[1,2], is believed to be a driving force behind the rich phase diagram of many correlated electronic systems[3–5]. This paper explores the connection between the quasiparticles and collective modes in a doped antiferromagnet within the framework of local dynamical mean field theory (DMFT)[6]. It is known that local DMFT is not fully capable of addressing the effects of non-local correlation, which are particularly important for the critical phenomena in low-dimensional system. In this paper, however, we aim to investigate to what extent local DMFT can depict the spin fluctuations in a strongly correlated system and the possibility to construct the non-local effects from local DMFT. In fact, the formalism for two-particle response functions, although proposed in the early stage of DMFT[6], has not been well explored to study the dynamical properties of two-particle fluctuations. Recently, an approach based on this formalism and random phase approximation (RPA) has gained success in describing the magnetic excitations in iron pnictides[7–9]. In this work, we make a step beyond the RPA approach by taking full account of the frequency dependence of the vertex functions, and compute the momentum dependence of excitation energy and damping rate of spin fluctuations, in hope of providing insight and guidance in interpreting the spectra of correlated materials from neutron and resonant inelastic X-ray scattering measurements (RIXS)[10–16].

With the two-dimensional Hubbard model as a working example, we use the vertex functions to calculate the non-local correction to the single electron self energy in the leading order of quasiparticle-paramagnon interaction. We show that the leading order correction reproduces the momentum-dependent feature that emerges from self-consistent calculation in cluster extensions of DMFT[17–19]. We also compare it with the non-local correction obtained by the phenomenological approach based on the Spin-Fermion (SF) model[20,21] where the vertices are replaced by constants. The result highlights the importance of energy dependence in the interaction
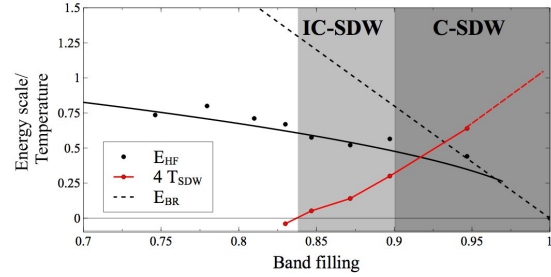

FIG. 1. The energy scales and the phase diagram of the doped Hubbard model at $T = 0.02$. E_{HF} is the characteristic energy scale for the frequency dependence of the self energy. The solid line is a guide for the eye. $E_{BR} = (1-n)W$ is the Brinkman-Rice scale. T_{SDW} is the SDW transition temperature. Shading highlights regions with commensurate (C) or incommensurate (IC) SDW ordering vector $\mathbf{Q}_{SDW}$.

vertices to capture the non-local physics in a perturbative approach.

We study the two-dimensional Hubbard Hamiltonian on a square lattice with nearest t and next nearest neighbor hopping t',

$$H = -\sum_{\langle i,j\rangle,\sigma} t_{ij} c_{i,\sigma}^{\dagger} c_{j,\sigma} + U \sum_i c_{i\uparrow}^{\dagger} c_{i\uparrow} c_{i\downarrow}^{\dagger} c_{i\downarrow}. \quad (1)$$

Taking $t = 1$ as the unit for energy and temperature, we set $t' = -0.3$ and the Coulomb interaction $U = 14$. The non-interacting bandwidth is $W = 8$. We focus on the band fillings between $n = 0.6$ and $n = 0.9$. To solve the effective impurity problem in the DMFT self-consistent condition we adopt the continuous time quantum Monte Carlo (CTQMC) method[22] as implemented in Ref.[23].

Figure 1 presents a summary of the main results. Near half filling, the model undergoes a spin density wave (SDW) transition and the transition temperature T_{SDW} decreases as more holes are introduced. The ordering vector for $n \geq 0.9$ is commensurate (C), $\mathbf{Q}_{SDW} = (\pi, \pi)$. When $n < 0.9$, $\mathbf{Q}_{SDW}$ becomes incommensurate (IC)
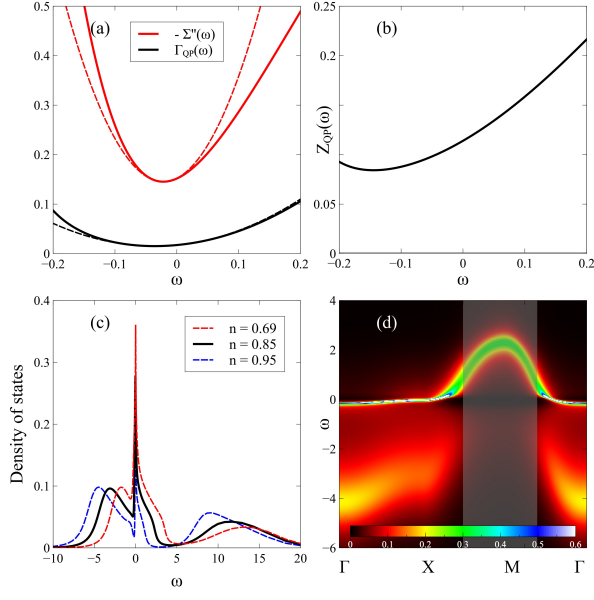
FIG. 2. Spectral properties for $n = 0.85$ and $T = 0.02$. (a) The imaginary part of the self energy $-\Sigma''(\omega)$ and the QP damping $\Gamma_{QP}(\omega)$. The dashed lines represent a quadratic fit in the region $|\omega| \leq 0.05$. (b) The quasiparticle residue $Z_{QP}(\omega)$. (c) The density of states (DOS). Also shown are the DOS for $n = 0.69$ and $n = 0.95$. (d) The spectral function $A_{\mathbf{k}}(\omega) = -G_{\mathbf{k}}''(\omega)/\pi$.
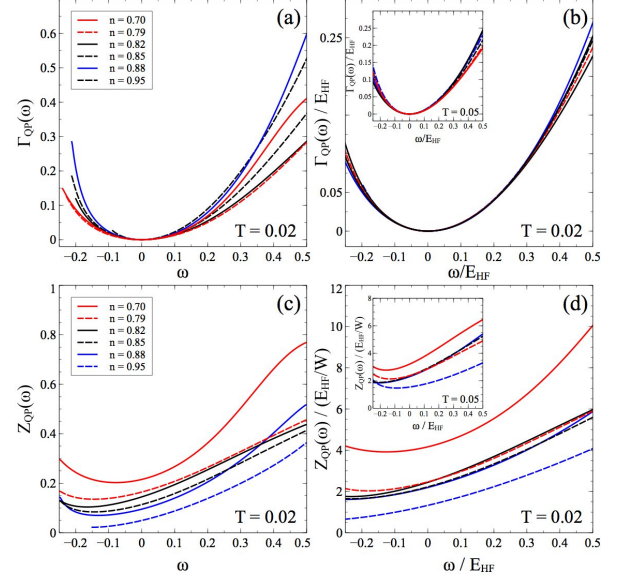
FIG. 3. (a) The QP damping rate; (b) the QP damping rescaled by the renormalized Fermi energy E_{HF} of the hidden QPs; (c) the QP residue; (d) the QP residue rescaled by E_{HF}. Main panels: $T = 0.02$. Inset in (b) and (d): $T = 0.05$.

and at $n \simeq 0.84$, T_{SDW} vanishes, defining the quantum critical point (QCP). In the vicinity of the QCP ($0.76 \lesssim n \lesssim 0.9$), the frequency dependent part of the Green's function $\omega - \Sigma(\omega)$ can be fit by a universal function of ω/E_{HF} (see Eq. (2)), where E_{HF} is the effective Fermi energy characterizing the energy dependence of quasiparticle (QP) damping rate. Near QCP, E_{HF} deviates from the Brinkman-Rice scale $E_{BR} = (1-n)W$[24], which is the Fermi energy in a slightly doped Mott insulator in the strong coupling limit. The self energy also leads to strong energy dependence in the QP residue Z_{QP} in this region ($0.76 \lesssim n \lesssim 0.9$), which is not described by a conventional Landau–Fermi liquid theory.

The single electron Green's function. The Hubbard model has been investigated extensively by the DMFT community[6,17,18,25], with the most attention focused on the single electron Green's function $G_{\mathbf{k}}(\omega)$ and the density of states. Since the Green's function is also an important ingredient of the SF model, we are compelled to discuss it first. We start with the local self energy.

The physical meaning of E_{HF} can be grasped from Figure 2(a): it is the energy scale below which a band of heavy fermions is formed. These fermions can be considered as QPs, as at small frequencies $|\omega| < E_{HF}$ their damping rate is quadratic in frequency: $\Gamma_{QP}(\omega) = -Z_{QP}\Sigma'' \sim (\omega/E_{HF})^2$. The self energy $\Sigma(\omega)$ itself is quadratic only in a very narrow range of frequencies: $|\omega| \lesssim \omega^* = 0.05$. A strong frequency dependence of $Z_{QP} = (1 - d\Sigma'(\omega)/d\omega)^{-1}$, as shown in Figure 2(b), helps

the QPs to remain well defined in the entire frequency interval below E_{HF}. The dashed lines in Figure 2(a) are quadratic fits of $\Gamma(\omega)$ and $\Sigma''(\omega)$, suggesting the robustness of the QPs far beyond ω^*. We point out ω^* is the energy scale for "kink" structure[26] in the spectral function. For $\omega < \omega^*$, the QP dispersion is renormalized by $Z_{QP} \simeq (1 - n) = E_{BR}/W$. When $|\omega| > \omega^*$, Z_{QP} continuously deviates from $(1 - n)$, and so does the QP band renormalization. E_{HF} ensures the QPs remains resilient beyond ω^*. Also noteworthy from the fitting is that the electron-like QPs ($\omega > 0$) extends to $\omega \simeq 0.2$, while hole-like ($\omega < 0$) only to $\omega \simeq -0.13$. The strong energy/temperature dependence in Z_{QP} has given rise to the concept of hidden Fermi liquid (HFL)[27–29], in which the linear resistivity and other anomalous transport properties of correlated metals are consequences of the strong temperature dependence of Z_{QP}, but the QPs remain well defined such that transport can be treated with the Boltzmann theory.

In our effort to determine the degree of universality present in the Hubbard model we fit the frequency dependent part of the Green's function by the scaling form:

$$\omega - \tilde{\Sigma}(\omega) = W \times g(\omega/E_{HF}), \qquad (2)$$

where $\tilde{\Sigma}(\omega) = \Sigma(\omega) - \Sigma(\omega = 0)$. As illustrated by Figure 3(b) and (d), this scaling works very well in the vicinity of the QCP, namely, for the interval $0.79 < n < 0.88$, and for $|\omega| < E_{HF}/2$. We point out that Eq. (2) is different from the scaling form near the Mott insulating state proposed by a renormalization group study in Ref.[30], where the scaling is controlled by E_{BR}.

The strong ω-dependence of Z_{QP} leads to strong momentum dependency of the QP residue. The latter fact enables us to explain the famous "waterfall" phenomenon observed in angular-resolved photoemission experiments[31–34]. This phenomenon amounts to vanishing of the spectral weight in the lower Hubbard band in a particular region of the Brillouin zone. In the strong coupling limit ($U \to \infty$), the high energy excitations with double occupancy (the upper Hubbard band) carry spectral weight of $n/2$[35]. Therefore the combined spectral weight for the QPs and the lower Hubbard band is $1-n/2$ (Figure 2(c)). In the shaded region of Figure 2(d) the QPs with $\omega > 0.5$ exhaust all available spectral weight leaving nothing for the states below the chemical potential. Approaching the Fermi surface Z_{QP} decreases, giving rise to the kink in the QP dispersion and the emergence of the incoherent continuum. The incoherent continuum at $\omega < -2$ is placed around the bare band dispersion and is connected to the QP band by the spectral intensity in the vertical direction (the "waterfall").

We see that the high energy waterfall feature, along with the low energy "kink" feature[26] in the QP band, is a consequence of the ω-dependent self energy which is characterized by a single energy scale E_{HF}. As far as we are aware, this connection has not been addressed in previous works[36–41].

Lattice susceptibilities in the spin channel. Computing the lattice susceptibility of bosonic modes within local DMFT requires an extra effort[6]. Firstly, one needs to determine the local irreducible vertex in the spin ('S') channel $\Gamma_{irr}^S(i\nu, i\nu')_{i\Omega}$. It is computed by the Bethe-Salpeter equation:

$$\left[\chi_{loc}^S(i\nu, i\nu')_{i\Omega}\right]^{-1}$$
$$= \left[\chi_{loc}^0(i\nu, i\nu')_{i\Omega}\right]^{-1} + \frac{1}{\beta^2}\Gamma_{irr}^S(i\nu, i\nu')_{i\Omega}, \quad (3)$$

where $\chi_{loc}^S(i\nu, i\nu')_{i\Omega}$ is the local two-particle correlation function in the spin channel and $\chi_{loc}^0(i\nu, i\nu')_{i\Omega} = -\beta G_{loc}(i\nu)G_{loc}(i\nu+i\Omega)\delta_{\nu\nu'}$ is the local polarization bubble. $G_{loc}(i\nu)$ is the local Green's function fully dressed by the self energy. $\chi_{loc}^S(i\nu, i\nu')_{i\Omega}$ and $G_{loc}(i\nu)$ are sampled by the CTQMC solver.

The lattice (**q**-dependent) two-particle correlation function $\chi^S(i\nu, i\nu')_{\mathbf{q}, i\Omega}$ is constructed from $\Gamma_{irr}^S(i\nu, i\nu')_{i\Omega}$ and the **q**-dependent polarization bubble $\chi_0(i\nu, i\nu')_{\mathbf{q}, i\Omega} = -\beta \sum_{\mathbf{k}} G_{\mathbf{k}}(i\nu)G_{\mathbf{k}+\mathbf{q}}(i\nu + i\Omega)\delta_{\nu\nu'}$,

$$\left[\chi^S(i\nu, i\nu')_{\mathbf{q}, i\Omega}\right]^{-1}$$
$$= [\chi_0(i\nu, i\nu')_{\mathbf{q}, i\Omega}]^{-1} + \frac{1}{\beta^2}\Gamma_{irr}^S(i\nu, i\nu')_{i\Omega}, \quad (4)$$

The dynamical susceptibility in the Matsubara frequency domain is then calculated by closing the fermionic frequencies, $\chi^S(\mathbf{q}, i\Omega) = \frac{1}{\beta^2}\sum_{\nu,\nu'}\chi^S(i\nu, i\nu')_{\mathbf{q}, i\Omega}$. Finally, we fit $\chi(\mathbf{q}, i\Omega)$ by the damped harmonic model to determine the resonance energy $\Omega^S(\mathbf{q})$ and the damping rate
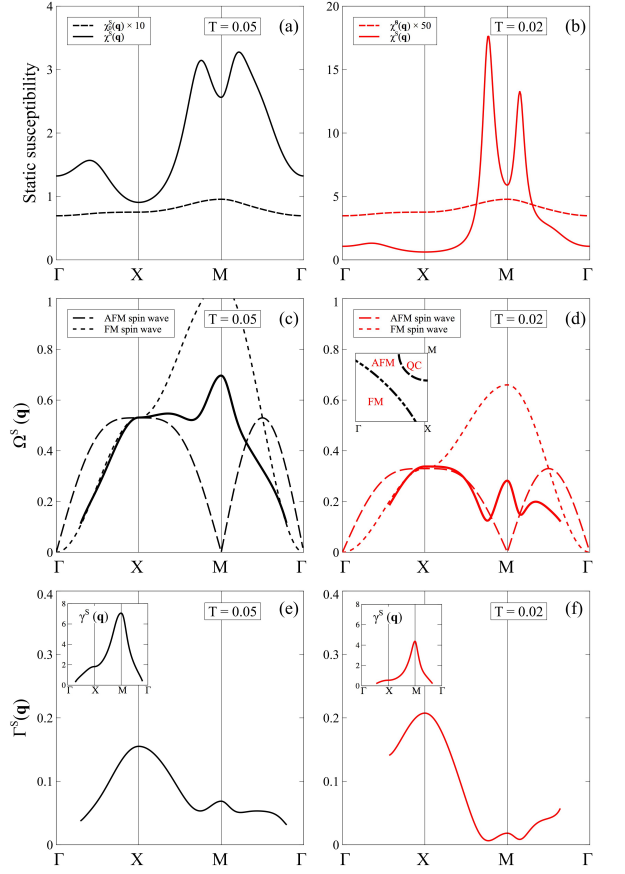

FIG. 4. (a) and (b): Static susceptibility at $T = 0.05$ and $T = 0.02$. Solid line: $\chi^S(\mathbf{q})$. Dashed line: $\chi_0^S(\mathbf{q})$ computed by the polarization bubble. $\chi_0^S(\mathbf{q})$ is multiplied by 10 or 50 for comparison. (c) and (d) Resonance energy $\Omega^S(\mathbf{q})$ and the dispersion of AFM and FM spin wave. Inset of (d): partition of the Brillioun zone by the nature of spin excitations. (e) and (f): The relaxation rate $\Gamma^S(\mathbf{q}) = (\Omega^S(\mathbf{q}))^2/\gamma^S(\mathbf{q})$ and damping rate $\gamma^S(\mathbf{q})$. $n = 0.85$.

$\gamma^S(\mathbf{q})$,

$$\chi^S(\mathbf{q}, i\Omega) = \frac{\chi^S(\mathbf{q})\Omega^S(\mathbf{q})^2}{\Omega^S(\mathbf{q})^2 + |\Omega|^2 + \gamma^S(\mathbf{q})|\Omega|} \quad (5)$$

where $\chi^S(\mathbf{q})$ is the static spin susceptibility at $\Omega = 0$. The analytical continuation to real frequencies is straightforward by taking $i\Omega \to \Omega + i0^+$ in the damped harmonic model. The RPA approach adopted in Ref.[7–9] approximates $\Gamma_{irr}^S(i\nu, i\nu')_{i\Omega}$ in Eq. (4) by a constant, while we retain the full frequency dependence of $\Gamma_{irr}^S(i\nu, i\nu')_{i\Omega}$.

Figure 4 shows details of spin dynamics in the damped harmonic model for $T = 0.05$ (left column) and $T = 0.02$ (right column). Figure 4 (a) and (b) compare the "bare" static susceptibility $\chi_0(\mathbf{q})$ (the polarization bubble) and the full static susceptibility $\chi^S(\mathbf{q})$. Without the vertex contribution, $\chi_0(\mathbf{q})$ is only weakly dependent on **q** and temperature, suggesting that the instability does not

originate from the particle-hole excitations at the Fermi surface. To find the SDW transition temperature for a given $\mathbf{q}$, we extrapolate $1/\chi^S(\mathbf{q})$ to zero as a function of T. Figure 4 (a) and (b) suggest those $\mathbf{q}$'s with most diverging $\chi^S(\mathbf{q})$ form a "ring" around the M point. Then we pick the $\mathbf{q}$ with the highest transition temperature T_{SDW} as the SDW ordering vector $\mathbf{Q}_{SDW}$, with T_{SDW} the SDW transition temperature of the system. Figure 1 shows the variation of T_{SDW} and $\mathbf{Q}_{SDW}$ with band filling. $\mathbf{Q}_{SDW} = (\pi, \pi)$ for $n \geq 0.9$ and is incommensurate for $n \leq 0.9$. For instance, for band filling $n = 0.85$, we have $\mathbf{Q}_{SDW} \simeq (\pi \pm 0.2\pi, \pi)$ and $(\pi, \pi \pm 0.2\pi)$. The QCP for the SDW order is located at $n \simeq 0.84$.

The damped harmonic model reveals the partition of the spin excitations in $\mathbf{q}$-space, as shown in Figure 4(c) and (d). Near the Γ point the resonance energy $\Omega^S(\mathbf{q})$ follows the dispersion of the ferromagnetic (FM) spin wave. Passing the X point and approaching the M point, $\Omega^S(\mathbf{q})$ traces the antiferromagnetic (AFM) spin wave at $T = 0.02$ and then enters the critical ring centered on the M point, where $\Omega^S(\mathbf{q})$ develops a "mexican hat" shape, with low-lying excitations located on the ring. The damping rate $\gamma^S(\mathbf{q})$ (inset of Figure 4(e) and (f)) is peaked at the M point, suggesting the FM paramagnons near Γ are only weakly damped. Passing the M point, the paramagnons become overdamped ($\Omega^S(\mathbf{q}) < \gamma^S(\mathbf{q})/2$). The low-lying critical incommensurate paramagnons, characterized by the relaxation rate $\Gamma^S(\mathbf{q}) \equiv (\Omega^S(\mathbf{q}))^2/\gamma^S(\mathbf{q})$, is shown in Figure 4 (e) and (f). The coexistence of incommensurate paramagnons at low energy and overdamped AFM fluctuations at high energy, along with the signature of FM fluctuations, resembles the spin dynamics in the normal state of cuprate superconductors as measured by neutron and RIXS experiments[10–16].

With the four-point correlation functions and vertex functions at hand we can calculate the non-local self energy due to the emission of paramagnons. Although a self-consistent calculation on the two-particle level requires an extended DMFT framework, such as the dynamical vertex approximation[17], the dual fermion approach[18,19], or the dynamical cluster approximation[42], the leading order in the $\mathbf{q}$-dependent two-particle full vertex (FV) function $\Gamma^{\uparrow\downarrow}_{\mathbf{k}\mathbf{k}'}(i\omega, i\omega')_{\mathbf{q},i\Omega}$, which can be written in terms of the full vertices $\Gamma^{S/C}(i\omega, i\omega')_{\mathbf{q},i\Omega}$ in the spin ('S') and charge ('C') channel, provides us with a convenient way to examine the effect of incommensurate
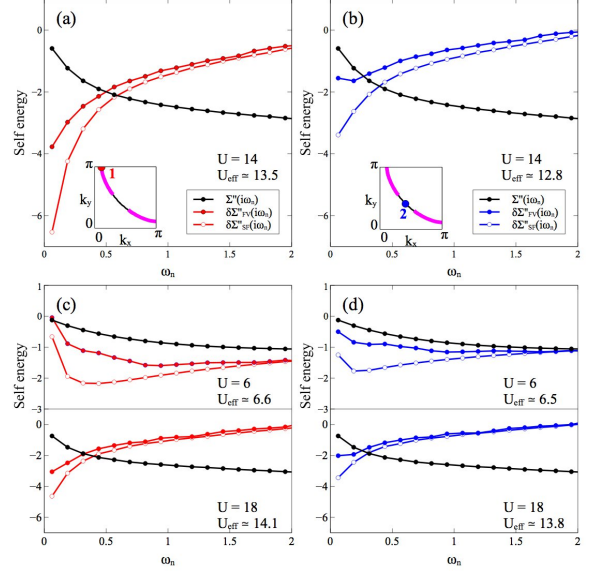

FIG. 5. Imaginary part of the self energy calculated with the full vertex (FV) functions and with spin-fermion (SF) models for antinodal point (**1**) and nodal point (**2**) for $U = 14$ in (a) and (b), $U = 6, 18$ in (c) and (d). Non-local corrections to the local self energy, $\delta\Sigma_{FV/SF}(\mathbf{k}, i\omega) = \Sigma_{FV/SF}(\mathbf{k}, i\omega) - \Sigma(i\omega)$ are presented with the local self energy $\Sigma(i\omega)$. Also shown are the values of the effective Coulomb interaction U_{eff} for the SF model (Eq. (9)). $n = 0.85$.

paramagnons,

$$
\begin{aligned}
&\Sigma_{\text{FV}}(\mathbf{k}, i\omega) \\
&= \frac{1}{2}Un - \frac{U}{\beta^2}\sum_{\omega',\Omega,\mathbf{q},\mathbf{k}'} G_{\mathbf{k}'+\mathbf{q}}(i\omega' + i\Omega)G_{\mathbf{k}'}(i\omega') \\
&\quad \times G_{\mathbf{k}+\mathbf{q}}(i\omega + i\Omega)\Gamma^{\uparrow\downarrow}_{\mathbf{k}\mathbf{k}'}(i\omega, i\omega')_{\mathbf{q},i\Omega} \\
&= \frac{1}{2}Un + \frac{U}{2\beta^3}\sum_{\omega',\Omega,\mathbf{q}} \chi_0(i\omega', i\omega')_{\mathbf{q},i\Omega}G_{\mathbf{k}+\mathbf{q}}(i\omega + i\Omega) \\
&\quad \times \big[3\Gamma^S(i\omega, i\omega')_{\mathbf{q},i\Omega} - \Gamma^C(i\omega, i\omega')_{\mathbf{q},i\Omega} \\
&\quad\quad + \Gamma^C_{loc}(i\omega, i\omega')_{i\Omega} - \Gamma^S_{loc}(i\omega, i\omega')_{i\Omega}\big]. \quad (6)
\end{aligned}
$$

We point to Ref.[17] and reference therein for the derivation of Eq. (6). The Feynman diagram for $\Sigma_{\text{FV}}(\mathbf{k}, i\omega)$ is sketched in Figure 6 (a). The full vertices $\Gamma^{S/C}(i\omega, i\omega')_{\mathbf{q},i\Omega}$ are calculated from the irreducible local vertex functions $\Gamma^{S/C}_{irr}(i\omega, i\omega')_{i\Omega}$ via

$$
\begin{aligned}
&\left[\frac{1}{\beta^2}\Gamma^{S/C}(i\omega, i\omega')_{\mathbf{q},i\Omega}\right]^{-1} \\
&= \left[\frac{1}{\beta^2}\Gamma^{S/C}_{irr}(i\omega, i\omega')_{i\Omega}\right]^{-1} - \chi_0(i\omega, i\omega')_{\mathbf{q},i\Omega}. \quad (7)
\end{aligned}
$$

Instead of isolated hot spots, the soft paramagnon fluctuations connect continuous segments of the Fermi surface, forming a hot region marked by purple in the in-
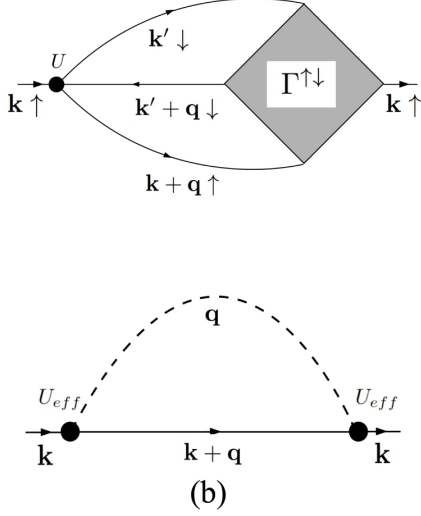
FIG. 6. Feynman diagrams for the self energy with (a) full vertices (FV) and with (b) the Spin-Fermion (SF) model.

set of Figure 5(a) and (b). We depict the local self energy $\Sigma''(i\omega)$ and the non-local correction $\delta\Sigma''_{FV}(\mathbf{k}, i\omega) = \Sigma''_{FV}(\mathbf{k}, i\omega) - \Sigma''(i\omega)$ calculated by Eq. (6) for $\mathbf{k}$'s at the antinodal point (**1**) and the nodal point (**2**) in Figure 5. For comparison, we also show the non-local correction calculated with the dynamical susceptibility $\chi^S(\mathbf{q}, i\Omega)$,

$$\delta\Sigma''_{SF}(\mathbf{k}, i\omega) = \Sigma''_{SF}(\mathbf{k}, i\omega) - \Sigma''(i\omega), \qquad (8)$$

where

$$\Sigma_{\mathrm{SF}}(\mathbf{k}, i\omega) = \frac{U_{eff}^2}{\beta} \sum_{\Omega, \mathbf{q}} \chi^S(\mathbf{q}, i\Omega) G_{\mathbf{q}+\mathbf{k}}(i\Omega + i\omega), \quad (9)$$

as is done in the Spin-Fermion (SF) model[20,21]. The Feynman diagram for $\Sigma_{SF}(\mathbf{k}, i\omega)$ is shown in Figure 6 (b). The effective Coulomb interaction U_{eff} is chosen to get the best fit to the $\Sigma''_{FV}(\mathbf{k}, i\omega)$ at high frequency.

Figure 5 shows the results for $U = 6, 14$, and 18. The FV and SF calculations lead to diminishing high frequency tails at both antinodal and nodal point, indicating that the non-local correction is significant only at low energy. At large $U = 14, 18$ the difference between the FV and SF results becomes quite pronounced at small energies. Although in both FV and SF model the self energy shows strong frequency dependence, the momentum dependence is different. At the nodal point, the energy dependence of $\delta\Sigma''_{FV}(\mathbf{k}, i\omega)$ resembles that of a Fermi liquid, while at the antinodal point, $\delta\Sigma''_{FV}(\mathbf{k}, i\omega)$ gives strong scattering. It is noteworthy that this momentum dependence of $\delta\Sigma''_{FV}(\mathbf{k}, i\omega)$ also emerges from recent calculations using dynamical cluster approximation[43], suggesting the leading order in the vertex functions captures the essential physics of the quasiparticle-paramagnon interaction. On the other hand, the SF model, which does not take into account the frequency dependence of the vertex function, overestimates the scattering in $\delta\Sigma''(\mathbf{k}, i\omega)$ at both antinodal and nodal point. It should also be noted that to achieve the convergence between the FV and the SF at high energy we need to adopt a very large value for U_{eff}. Admittedly, the success of the SF approach[20,21,44] should not be underestimated by a first order perturbative calculation in Eq. (9). By the comparison demonstrated in Figure 5, we emphasize that the two-particle approach based on vertex calculations in local DMFT is a convenient starting point to study the dynamics of spin fluctuations in correlated materials, given the availability of numerical packages[23,45] combining local DMFT and first principles methods, and their success in predicting the electronic structures of various correlated materials[46–49].

Conclusions. Using the example of the Hubbard model, we have demonstrated how the standard DMFT procedure can be augmented by the inclusion of corrections from interactions of quasiparticles with collective excitations. Our calculation points to the pivotal role of incommensurate critical paramagnons in a doped antiferromagnet, making contact with recent neutron scattering and RIXS measurements[10–14]. Such corrections become significant near the QCP, as predicted by the phenomenological SF model. Our calculations indicates that the frequency dependence of the interaction vertices is necessary to capture the non-local corrections.

[1] J. A. Hertz, Phys. Rev. B **14**, 1165 (1976).

[2] A. J. Millis, Phys. Rev. B **48**, 7183 (1993).

[3] B. Keimer, S. Kivelson, M. Norman, S. Uchida, and J. Zaanen, Nature **518**, 179 (2015).

[4] P. Coleman, "Heavy fermions: Electrons at the edge of magnetism," in *Handbook of Magnetism and Advanced Magnetic Materials* (John Wiley and Sons, Ltd, 2007).

[5] P. Dai, Rev. Mod. Phys. **87**, 855 (2015).

[6] A. Georges, G. Kotliar, W. Krauth, and M. J. Rozenberg, Rev. Mod. Phys. **68**, 13 (1996).

[7] H. Park, K. Haule, and G. Kotliar, Phys. Rev. Lett. **107**, 137007 (2011).

[8] M. Liu, L. W. Harriger, H. Luo, M. Wang, R. Ewings, T. Guidi, H. Park, K. Haule, G. Kotliar, S. Hayden, *et al.*, Nature Physics **8**, 376 (2012).

[9] Z. Yin, K. Haule, and G. Kotliar, Nature Physics **10**, 845 (2014).

[10] V. Hinkov, P. Bourges, S. Pailhes, Y. Sidis, A. Ivanov, C. Frost, T. Perring, C. Lin, D. Chen, and B. Keimer, Nature Physics **3**, 780 (2007).

[11] B. Vignolle, S. Hayden, D. McMorrow, H. Rønnow, B. Lake, C. Frost, and T. Perring, Nature Physics **3**, 163 (2007).

[12] D. Reznik, J.-P. Ismer, I. Eremin, L. Pintschovius, T. Wolf, M. Arai, Y. Endoh, T. Masui, and S. Tajima, Phys. Rev. B **78**, 132503 (2008).

[13] G. Xu, G. Gu, M. Hücker, B. Fauqué, T. Perring, L. Regnault, and J. Tranquada, Nature Physics **5**, 642 (2009).

[14] M. Le Tacon, G. Ghiringhelli, J. Chaloupka, M. M. Sala, V. Hinkov, M. Haverkort, M. Minola, M. Bakr, K. Zhou, S. Blanco-Canosa, *et al.*, Nature Physics **7**, 725 (2011).

[15] C. Jia, E. Nowadnick, K. Wohlfeld, Y. Kung, C.-C. Chen, S. Johnston, T. Tohyama, B. Moritz, and T. Devereaux, Nature communications **5** (2014).

[16] M. Dean, G. Dellea, R. Springell, F. Yakhou-Harris, K. Kummer, N. Brookes, X. Liu, Y. Sun, J. Strle, T. Schmitt, *et al.*, Nature Materials **12**, 1019 (2013).

[17] A. Toschi, A. A. Katanin, and K. Held, Phys. Rev. B **75**, 045118 (2007).

[18] A. N. Rubtsov, M. I. Katsnelson, and A. I. Lichtenstein, Phys. Rev. B **77**, 033101 (2008).

[19] A. N. Rubtsov, M. I. Katsnelson, A. I. Lichtenstein, and A. Georges, Phys. Rev. B **79**, 045133 (2009).

[20] A. Abanov and A. V. Chubukov, Phys. Rev. Lett. **84**, 5608 (2000).

[21] A. Abanov, A. V. Chubukov, and J. Schmalian, Advances in Physics **52**, 119 (2003).

[22] P. Werner, A. Comanac, L. de' Medici, M. Troyer, and A. J. Millis, Phys. Rev. Lett. **97**, 076405 (2006).

[23] K. Haule, Phys. Rev. B **75**, 155113 (2007).

[24] W. F. Brinkman and T. M. Rice, Phys. Rev. B **2**, 4302 (1970).

[25] H. Park, K. Haule, and G. Kotliar, Phys. Rev. Lett. **101**, 186403 (2008).

[26] K. Byczuk, M. Kollar, K. Held, Y.-F. Yang, I. Nekrasov, T. Pruschke, and D. Vollhardt, Nature Physics **3**, 168 (2007).

[27] W. Xu, K. Haule, and G. Kotliar, Phys. Rev. Lett. **111**, 036401 (2013).

[28] X. Deng, J. Mravlje, R. Žitko, M. Ferrero, G. Kotliar, and A. Georges, Phys. Rev. Lett. **110**, 086401 (2013).

[29] X. Deng, A. Sternbach, K. Haule, D. N. Basov, and G. Kotliar, Phys. Rev. Lett. **113**, 246404 (2014).

[30] P. Mai, H. Krishna-murthy, and B. S. Shastry, Annals of Physics , (2016), in press.

[31] J. Graf, G.-H. Gweon, K. McElroy, S. Y. Zhou, C. Jozwiak, E. Rotenberg, A. Bill, T. Sasagawa, H. Eisaki, S. Uchida, H. Takagi, D.-H. Lee, and A. Lanzara, Phys. Rev. Lett. **98**, 067004 (2007).

[32] D. S. Inosov, J. Fink, A. A. Kordyuk, S. V. Borisenko, V. B. Zabolotnyy, R. Schuster, M. Knupfer, B. Büchner, R. Follath, H. A. Dürr, W. Eberhardt, V. Hinkov, B. Keimer, and H. Berger, Phys. Rev. Lett. **99**, 237002 (2007).

[33] H. Iwasawa, Y. Yoshida, I. Hase, K. Shimada, H. Namatame, M. Taniguchi, and Y. Aiura, Phys. Rev. Lett. **109**, 066404 (2012).

[34] T. Das, T. Durakiewicz, J.-X. Zhu, J. J. Joyce, J. L. Sarrao, and M. J. Graf, Phys. Rev. X **2**, 041012 (2012).

[35] J. Hubbard, Proceedings of the Royal Society of London A: Mathematical, Physical and Engineering Sciences **276**, 238 (1963).

[36] A. Macridin, M. Jarrell, T. Maier, and D. J. Scalapino, Phys. Rev. Lett. **99**, 237001 (2007).

[37] C. Weber, K. Haule, and G. Kotliar, Phys. Rev. B **78**, 134519 (2008).

[38] Q. Yin, A. Gordienko, X. Wan, and S. Y. Savrasov, Phys. Rev. Lett. **100**, 066406 (2008).

[39] S. Chakraborty, D. Galanakis, and P. Phillips, Phys. Rev. B **78**, 212504 (2008).

[40] S. Sakai, Y. Motome, and M. Imada, Phys. Rev. B **82**, 134505 (2010).

[41] S. Fuchs, E. Gull, M. Troyer, M. Jarrell, and T. Pruschke, Phys. Rev. B **83**, 235113 (2011).

[42] M. H. Hettler, M. Mukherjee, M. Jarrell, and H. R. Krishnamurthy, Phys. Rev. B **61**, 12739 (2000).

[43] O. Gunnarsson, T. Schäfer, J. P. F. LeBlanc, E. Gull, J. Merino, G. Sangiovanni, G. Rohringer, and A. Toschi, Phys. Rev. Lett. **114**, 236402 (2015).

[44] Y. Wang and A. Chubukov, Phys. Rev. B **90**, 035149 (2014).

[45] K. Haule, Phys. Rev. Lett. **115**, 196403 (2015).

[46] J. Shim, K. Haule, and G. Kotliar, Nature **446**, 513 (2007).

[47] K. Haule, J. H. Shim, and G. Kotliar, Phys. Rev. Lett. **100**, 226402 (2008).

[48] K. Haule and G. Kotliar, Nature Physics **5**, 796 (2009).

[49] H. Park, A. J. Millis, and C. A. Marianetti, Phys. Rev. Lett. **109**, 156402 (2012).